The Binding of Bis-ANS to the Isolated GroEL Apical Domain Fragment Induces the Formation of a Folding Intermediate with Increased Hydrophobic Surface Not Observed in Tetradecameric GroEL†

Alison L. Smoot,‡ Markandeswar Panda,‡ Bill T. Brazil,‡ Ashley M. Buckle,§ Alan R. Fersht,§ and Paul M. Horowitz*,‡

Department of Biochemistry, University of Texas Health Science Center at San Antonio, San Antonio, Texas 78229-3900, and Cambridge University Chemical Laboratory and Cambridge Center for Protein Engineering, Medical Research Council Center, Hills Road, Cambridge CB2 2QH, U.K.

Received August 3, 2000; Revised Manuscript Received February 5, 2001

ABSTRACT: The extent of hydrophobic exposure upon bis-ANS binding to the functional apical domain fragment of GroEL, or minichaperone (residues 191−345), was investigated and compared with that of the GroEL tetradecamer. Although a total of seven molecules of bis-ANS bind cooperatively to this minichaperone, most of the hydrophobic sites were induced following initial binding of one to two molecules of probe. From the equilibrium and kinetics studies at low bis-ANS concentrations, it is evident that the native apical domain is converted to an intermediate conformation with increased hydrophobic surfaces. This intermediate binds additional bis-ANS molecules. Tyrosine fluorescence detected denaturation demonstrated that bis-ANS can destabilize the apical domain. The results from (i) bis-ANS titrations, (ii) urea denaturation studies in the presence and absence of bis-ANS, and (iii) intrinsic tyrosine fluorescence studies of the apical domain are consistent with a model in which bis-ANS binds tightly to the intermediate state, relatively weakly to the native state, and little to the denatured state. The results suggest that the conformational changes seen in apical domain fragments are not seen in the intact GroEL oligomer due to restrictions imposed by connections of the apical domain to the intermediate domain and suppression of movement due to quaternary structure.

Mature proteins must assume unique three-dimensional conformations to gain their native functions. Some smaller proteins can fold into their native conformations without any assistance. However, along the folding pathway, larger proteins may expose extensive hydrophobic patches in an attempt to reach the native structure. In the highly condensed environments of the cell, these exposed hydrophobic patches tend to favor aggregation and may lead to misfolding. A class of molecules known as molecular chaperones has been shown to assist in protein folding. The molecular chaperone GroEL assists in the in vitro and in vivo refolding of a number of proteins (*1*−*5*), and it interacts with over half of the proteins from *Escherichia coli* (*6*). GroEL is composed of 14 identical 57 kDa subunits arranged in 2, 7-subunit rings (7mers), which form a double-ring complex that encloses a central cavity in each ring (*7*). The GroEL crystal structure demonstrates that each GroEL subunit is made up of three domains: the equatorial domain, the intermediate domain, and the apical domain (*8*−*10*). The equatorial domain is the site of nucleotide binding and is responsible for making most of the side-to-side contacts within the 7mer ring and all of the contacts between the two stacked rings of GroEL (*11*). The apical domain is the site of substrate polypeptide and GroES binding (*11*), which occurs at residues that face into the central channel (*12*). The intermediate domain connects the equatorial and apical domains and may play a role in allosteric communication between the two domains (*8*). From photoincorporation studies, it has been shown that the hydrophobic probe bis-ANS[1] binds in a region of the GroEL sequence (residues 204−249) that maps to the GroEL apical domain (residues 191−376) (*13, 14*).

In vitro experiments have shown that an initial step in the refolding by GroEL is the binding of the non-native peptide by the GroEL oligomer (*15*−*19*). This complexation prevents off-pathway events, such as degradation and aggregation, which decrease the efficiency of folding (*2, 20, 21*). In general, maximum folding by GroEL requires the intact central cavity of the oligomer (*22*−*24*), and, therefore, the complete double-ring system. However, a single-ring GroEL can be sufficient for folding certain proteins, in vivo (*25*). It has been shown that single rings cannot discharge bound GroES from the GroEL/GroES complex, and they are unable

† This work was supported by National Institutes of Health Grant GM25177 and Robert A. Welch Foundation Grant AQ723 (to P.M.H.).

* Address correspondence to this author at the Department of Biochemistry, University of Texas Health Science Center at San Antonio, Mail Code 7760, 7703 Floyd Curl Dr., San Antonio, TX 78229-3900. Phone: 210-567-3737, FAX: 210-567-6595, Email: Horowitz@biochem.uthscsa.edu.

‡ University of Texas Health Science Center at San Antonio.

§ Medical Research Council Center.

[1] Abbreviations: bis-ANS, 4,4′-bis(1-anilino-8-naphthalenesulfonic acid); DEAE, diethylaminoethyl cellulose; DTT, dithiothreitol; EDTA, ethylenediaminetetraacetic acid; Ni-NTA, nickel-nitrilotriacetic acid; SDS, sodium dodecyl sulfate.

10.1021/bi001822b CCC: $20.00
Published on Web 03/10/2001

to release folded proteins enclosed in the central cavity, but they can chaperone the folding of substrates which do not require GroES (*26*). Urea denaturation studies of GroEL found residual structure contained within the apical domain that might serve as an organized hydrophobic region capable of interacting with substrate polypeptides (*27*). Recently, it has been demonstrated that the unfolding and disassembly of GroEL in guanidine hydrochloride or urea occur through a tetradecameric intermediate with a folded equatorial domain but with unfolded apical and intermediate domains (*19*).

Fragments representing the apical domain of GroEL [sht-GroEL (191−345), sht-GroEL (191−376)] (*28*) have been cloned, and a proteolytically produced fragment [GroEL (150−456)] (*29, 30*) has been isolated. These fragments have been termed minichaperones, which show chaperone activity in vitro (*31*) and in vivo (*32*), but at slower rates and with looser binding when compared to the intact GroEL oligomer. The crystal structures of the minichaperones sht-GroEL (191−345) and sht-GroEL (191−376) are very similar to that of the apical domain in the intact GroEL (*33*). However, the stability and refolding activity of the isolated apical domain are considerably lower than those of the intact GroEL oligomer (*31, 32*). Thus, it is possible that the apical domain assists the refolding of substrate proteins, at least in part, by interacting with the exposed hydrophobic surfaces on the folding intermediate of the non-native polypeptides, thereby preventing aggregation (*21*). This hypothesis is based on the chaperone-like effect of bovine serum albumin in assisting the refolding of rhodanese, which would self-associate in its absence (*27*). The identification of peptide binding sites of the isolated minichaperones sht-GroEL (191−345) and sht-GroEL (191−376) in solution has been published recently (*21, 34*). NMR analysis (*35*) showed that the synthetic peptide (Rho), corresponding to the N-terminal α-helix residues 11−23 of mitochondrial rhodanese, specifically binds to sht-GroEL (191−345). Equilibrium and kinetic studies of the minichaperones sht-GroEL (191−345) and sht-GroEL (191−376) demonstrated reversible thermal unfolding and refolding (*31*).

In this report we used the apical domain fragment sht-GroEL (191−345) to understand the nature of an intermediate detected at saturating concentrations of bis-ANS (*31*). Equilibrium and kinetic binding of bis-ANS to the apical domain were followed by bis-ANS fluorescence, intrinsic tyrosine fluorescence, and circular dichroism.

MATERIALS AND METHODS

Reagents and Proteins. Electrophoresis quality urea was purchased from Bio-Rad. All other reagents were of analytical grade. Bis-ANS was purchased from Molecular Probes, Inc. (Eugene, OR). Ni-NTA[1] agarose was supplied by Qiagen (Hilden, Germany).

Bovine liver rhodanese was purified as previously described (*36*). GroES was purified from lysates of *E. coli* bearing the multicopy plasmid pND5 as described (*37*). The GroEL apical domain fragment (191−345) with the N-terminal histidine tag of 17 amino acids (-17 MRSGSHH-HHHHGLVPRGS -1) was purified from lysates of *E. coli* containing the pRSET A vector (Invitrogen) as described (*28*). All apical domain experiments were performed using the C-terminally truncated GroEL apical domain fragment 191−345 containing the 17 amino acid N-terminal tag.

The chaperonin GroEL was purified from lysates of *E. coli* bearing the multicopy plasmid pND5. The purification was a modified version of the previously described protocol (*37*). The lysate was made 65% in ammonium sulfate and dialyzed overnight in 50 mM Tris-HCl, pH 7.8, 0.5 mM DTT,[1] 0.1 mM EDTA[1] (Buffer A). Following dialysis, the sample was applied to a DEAE[1]-ion exchange column, and an increasing salt gradient (0−0.45 M NaCl) was used to elute the protein. GroEL fractions were collected and precipitated with ammonium sulfate. The precipitate was dissolved in 10 mL of Buffer A containing 50 mM NaCl, and the resulting solution was applied to a Sephacryl S-400 column equilibrated with Buffer A containing 50 mM NaCl. GroEL-containing fractions were precipitated with ammonium sulfate. The precipitate was then dissolved in 20 mL of Buffer A and dialyzed against 2 L of the same buffer. To remove any traces of remaining tryptophan contamination, ∼2−10 mg/mL GroEL was applied to a Reactive Red 120 agarose column according to a previously published protocol (*38*). The column was preequilibrated with Buffer A at 4 °C. The protein was equilibrated on the column for 15 min before elution with Buffer A. GroEL-containing fractions were identified by 12% SDS[1] gels. The purified GroEL was then dialyzed against 50 mM Tris-HCl (pH 7.8) containing 1 mM DTT. Glycerol was then added to 10% (v/v), and aliquots were frozen in liquid nitrogen and stored at −80 °C.

Sedimentation Analysis. Apical domain samples (5, 8, and 16 μM protein) were subjected to sedimentation velocity analysis at 25 °C using a Beckman XL-A analytical ultracentrifuge with a rotor speed of 60 000 rpm. Apical domain samples incubated with various concentrations of urea (0, 3.5, 5 M) were subjected to sedimentation velocity analysis under the conditions described above. The sedimentation boundary was monitored at 230 and 280 nm, which are the characteristic absorbances due to the peptide bond and aromatic side chains, respectively. The data were analyzed by the method of van Holde and Weischet (*39*) using the UltraScan ultracentrifuge data collection and analysis program (*40*). Subsequent analysis of the unlabeled apical domain in the absence of urea was performed by fitting the experimental data by the finite-element method (*40*) using a model for a single component system. The partial specific volume was estimated from the amino acid sequence using the method of Sober (*41*). The data were corrected for buffer viscosity and density.

Fluorescence Spectroscopy. The buffer used in all experiments was 10 mM sodium hydrogen phosphate (pH 7.0), the temperature was 25 °C, and all of the concentrations given are final concentrations. Bis-ANS fluorescence experiments were performed using a Fluorolog-3 spectrofluorometer (ISA, Inc.) with an excitation wavelength of 395 nm (slit width 2 nm) and an emission wavelength of 495 nm (slit width 5 nm). Emission spectra (Figure 1) of 1 mL solutions of 5 μM apical domain, 5 μM bis-ANS + 5 μM apical domain, 5 μM bis-ANS + 5 μM apical domain + 2.5 M urea, and 5 μM bis-ANS + 5 μM apical domain + 5.0 M urea were scanned from 440 to 510 nm. Appropriate blanks were subtracted from each scan.

Bis-ANS titrations were performed on 1 mL solutions of either 5 μM apical domain (Figure 3) or 0.357 μM GroEL oligomer (corresponds to 5 μM apical domain) (Figure 4).

The fluorescence intensities were corrected for the inner filter effect (*42*) and analyzed by nonlinear, least-squares fits using a modified form of the Hill equation:

$$F_{obs} = \frac{F_{max}[S]^n}{K' + [S]^n} \quad (1)$$

where F_{obs}, F_{max}, K', n, and [S] are the observed fluorescence intensity, maximum fluorescence intensity, binding constant, Hill coefficient, and bis-ANS concentration, respectively.

To estimate the number of moles of bis-ANS bound per protein, a reverse binding experiment was performed. In this experiment, a fixed amount of bis-ANS was titrated with an increasing amount of the protein. These data were then plotted as $1/F_{obs}$ versus 1/[protein] and extrapolated back to zero on the *x*-axis, which theoretically corresponds to infinite apical domain concentration. Bis-ANS fluorescence scans indicated that the peak at 495 nm did not shift with increasing bis-ANS concentration, suggesting that the quantum yields of the bound probe molecules are the same. This indicates that the fluorescence contribution of each bound bis-ANS molecule is equal. The fluorescence intensity derived from the *y*-intercept corresponds to the fluorescence when all of the initial bis-ANS is bound. These data permit the determination of bound bis-ANS from measurements of bis-ANS fluorescence intensity. These fluorescence measurements were used to obtain plots of $[\text{bis-ANS}]_{bound}$ vs $[\text{bis-ANS}]_{free}$ for the determination of the number of bis-ANS molecules bound at any given total bis-ANS concentration.

Circular Dichroism Spectroscopy. Circular dichroism spectra of the apical domain in 0−8 M urea at 25 °C in the far-UV (190−250 nm) region were collected using an OLIS DSM 16 UV/VIS CD Spectrophotometer (On Line Instrument Systems, Inc., Bogart, GA). A 1 mm path cylindrical cell (1 mL volume) was used. The scans were recorded at 2 s/data point. The experimental conditions were 10 mM Na_2HPO_4/NaH_2PO_4, pH 7, [protein] = 5 μM. The CD experiments for unfolding and refolding were performed after the solutions had been equilibrated for 24 h. For refolding experiments, the protein was unfolded for 5 h at 2 mg/mL in 8 M urea-containing buffers and then diluted into the buffers containing the calculated amounts of urea to give the desired final concentrations of urea. Buffer blanks were collected and subtracted from the appropriate sample spectra.

For the CD spectra reported in Figure 7, a 2 mm path length cylindrical cell (2.5 mL volume) was used. The data were recorded at 5 s/data point in the wavelength range 200−360 nm. The treatment of the apical domain in 3.0 M urea was done by equilibrating a 5 μM sample of the protein in 3.0 M urea for 24 h. The solution containing 5 μM protein and 30 μM bis-ANS was equilibrated for 5 h to ensure maximum binding. Appropriate blank spectra were recorded and subtracted from the sample spectra. The data below 200 nm were extremely noisy because of the high absorbance of the solutions in the presence of either urea or bis-ANS.

Apical Domain Denaturation. The urea denaturation of the apical domain was detected by bis-ANS fluorescence and intrinsic tyrosine fluorescence. Bis-ANS fluorescence was excited at a wavelength of 394 nm, and the emission was detected at 500 nm. The intrinsic tyrosine fluorescence was excited at a wavelength of 275 nm, and the emission was detected at 302 nm. To follow the denaturation of the apical domain by bis-ANS fluorescence, individual 1 mL solutions of the apical domain (5 μM) were incubated with increasing concentrations of urea (0−8.0 M) in the presence of either 1, 5, or 30 μM bis-ANS for either 30 min or 20 h at 25 °C, and the bis-ANS fluorescence intensities were measured. To follow the denaturation of the apical domain by tyrosine fluorescence, individual 1 mL samples of the apical domain (5 μM) were incubated with increasing concentrations of urea (0−8.0 M) in the absence or presence of 5 and 30 μM bis-ANS for 20 h at 25 °C, and the tyrosine fluorescence was subsequently measured. The parameters for the unfolding and refolding curves were obtained by nonlinear, least-squares analysis using the two-state equation (eq 2) (*43*). The two-state model (N ⇆ U) assumes that there are only two states of the protein being studied, the native state (N) and the unfolded state (U), and that there is no accumulation of detectable intermediates:

$$F_{obs} = \frac{[(y_f + m_f[D]) + (y_u + m_u[D])(\exp-\{\Delta G_{(H2O)}/RT - m[D]/RT\})]}{[1 + \exp-\{\Delta G_{(H2O)}/RT - m[D]/RT\}]} \quad (2)$$

where F_{obs} is the fluorescence observed, R is the gas constant (0.001987 kcal mol K^{-1}), T is the absolute temperature, [D] is the denaturant concentration, $\Delta G_{(H2O)}$ is the free energy in the absence of denaturant, y_f and m_f are the intercept and slope of the pre-transition baseline, respectively, y_u and m_u are the intercept and slope of the post-transition baseline, respectively, and m is the slope of the unfolding transition.

Additional attempts were made to fit the curve to a nonlinear, least-squares analysis using the three-state model. A three-state model (N ⇆ I ⇆ U) is used when a detectable intermediate (I) is involved:

$$F_{obs} = \frac{S_N + S_N K_{NI} + S_U K_{NI} K_{IU}}{1 + K_{NI} + K_{IU} + K_{NI} + K_{IU}} \quad (3)$$

$$K_{NI} = \exp\{-(\Delta G^\circ_{w,NI} + m_{NI}[U])/RT\} \quad (4)$$

$$K_{IU} = \exp\{-(\Delta G^\circ_{w,IU} + m_{IU}[U])/RT\} \quad (5)$$

where the subscripts "NI" and "IU" refer to the N ↔ I and I ↔ U equilibria, respectively. S_N, S_{NI}, and S_U are the fraction native signals for the native, intermediate, and unfolded states, respectively. Other parameters referring to these equilibria have similar meanings to those stated above. S_N, S_{NI}, S_U, $\Delta G^\circ_{w,NI}$, $\Delta G^\circ_{w,IU}$, m_{NI}, and m_{IU} were floated during the nonlinear least-squares regression of the data (*44*). Further details on the equations (eqs 3−5) can be found in the literature (*44*).

Bis-ANS Binding Kinetics. The kinetics of bis-ANS binding to the apical domain were performed with an excitation wavelength of 394 nm (2.5 nm slit width) and an emission wavelength of 500 nm (10 nm slit width) at 25 °C. Samples of 5 μM apical domain (3 mL) in 10 mM sodium hydrogen phosphate were stirred in a 1 cm path length cuvette. Subsequently, 1−50 μM aliquots of bis-ANS (final concentration) were added to the cuvette, and the bis-ANS fluorescence intensity at each bis-ANS concentration was measured as a function of time. To determine the rate

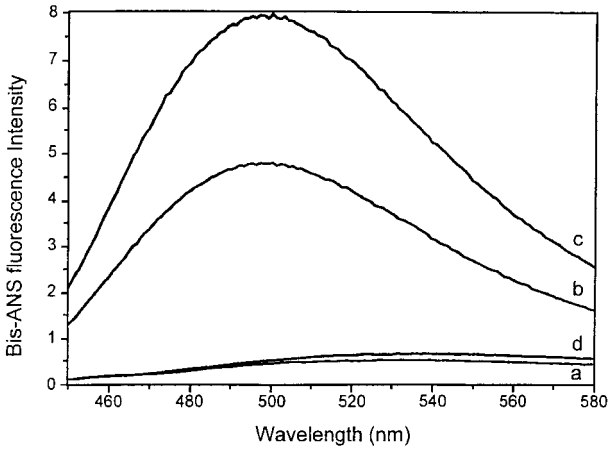

FIGURE 1: Bis-ANS fluorescence emission spectra. Fluorescence emission spectra of (a) bis-ANS (5 μM), (b) bis-ANS (5 μM) + apical domain (5 μM), (c) bis-ANS (1 μM) + apical domain (5 μM) + urea (2.5 M), and (d) bis-ANS (5 μM) + apical domain (5 μM) + urea (5.0 M), all in a 10 mM sodium phosphate buffer, pH 7.0.

of bis-ANS binding to the apical domain intermediate, 40 μM bis-ANS was added to a 5 μM apical domain sample (3 mL) that was incubated in 2.5 M urea, and the bis-ANS fluorescence intensity was measured as a function of time. The bis-ANS kinetic binding data for the slower phase were fit to a single-exponential first-order reaction by the equation:

$$A(t) = A_0 \cdot e^{-kt} + A(\infty) \quad (6)$$

where $A(t)$ and $A(\infty)$ are intensities of bis-ANS at time t and at equilibrium, respectively, while A_0 is the intensity at the beginning of the reaction, and k is the first-order rate constant. To estimate the initial bis-ANS fluorescence, amplitudes for the burst phase were obtained from the start of the second phase. Because of the fewer number of data points for the burst phase, it was not possible to fit the entire set of data to a biphasic equation.

RESULTS

Bis-ANS Binding Studies of the Apical Domain. The hydrophobic binding properties of the GroEL apical domain (191−345) were assessed by bis-ANS titration. The sensitivity of bis-ANS fluorescence to its environment makes it an excellent fluorescence probe for measuring hydrophobic binding interactions. Bis-ANS is a fluorescent probe that has a low quantum yield (i.e., fluorescence intensity) in polar environments, with a wavelength maximum of 550 nm. However, the binding of bis-ANS (5 μM) to hydrophobic surfaces of the apical domain (5 μM) results in both an increase in its quantum yield and a shift in the fluorescence wavelength maximum to 500 nm (Figure 1, spectrum b).

In this study, at low bis-ANS concentrations the apical domain intermediate demonstrated increased bis-ANS binding at ~2.5 M urea (see below), with a wavelength maximum of 500 nm (Figure 1, spectrum c). The bis-ANS fluorescence wavelength maximum of the apical domain intermediate (500 nm, Figure 1, spectrum c) does not differ from the bis-ANS wavelength maximum in the presence of the native apical domain (500 nm, Figure 1, spectrum b). This suggests that the bis-ANS binding environment of a probe bound to either the native or the intermediate structure has not changed, and the 1.7-fold increase in the fluorescence intensity is a result of the apical domain intermediate binding more molecules of bis-ANS than the native apical domain. The unfolding of the apical domain in 5.0 M urea (Figure 1, spectrum d) resulted in a loss of bis-ANS hydrophobic binding sites, indicated by the decrease in bis-ANS fluorescence and a shift of the wavelength maximum to 550 nm.

Apical Domain Sedimentation Velocity Analysis. Sedimentation velocity data were first analyzed by the method of van Holde and Weischet (*39*). This analysis resulted in a symmetric, vertical extrapolation plot, which showed a single S-value of 1.82×10^{-13} s for the apical domain in the absence of urea (data not shown). The integral distribution plot was essentially vertical for all three sets of data ($A_{230} = 0.4$, $A_{280} = 0.4$, $A_{280} = 0.8$), thus indicating a single species (*45*), in agreement with previously published crystallographic studies (*33*). A single S-value for the apical domain in 3.5 M urea was unobtainable due to the wide spread of data [$(0.8-1.82) \times 10^{-13}$ s]. This is expected for a partially unfolded protein with increased hydrophobic exposure, which would lead to increased interactions, but not the formation of large aggregates, that would increase the spread of the measured S-values. Samples containing either 5 or 8 M urea could not be analyzed due to very high absorbances of these solutions.

Subsequent fitting of the experimental data with the finite-element method (*45*) using a model for a single-component, ideal system resulted in an S-value of 1.82×10^{-13} s for the apical domain in the absence of urea, which is in excellent agreement with the results obtained from the van Holde−Weischet analysis. The diffusion coefficient was determined to be 9.59×10^{-7} cm^2/s. Using these sedimentation and diffusion coefficients, the frictional coefficient was calculated to be 4.22×10^{-8} g/s, the Stokes radius was determined to be 22.38 Å, and the minimum radius for the apical domains was calculated to be 17.47 Å. Using the X-ray structure (*32*), we determined from the volume and by measuring and averaging five dimensions of the apical domain, that the unhydrated radius of the particle was 17 Å. Thus, the minimal radius (17.47 Å), which refers to an unhydrated sphere with a molecular weight corresponding to the apical domain, is in good agreement with the crystallographic results of Buckle et al. (*33*). The hydration of the apical domain and the asymmetry introduced by the histidine tag that were not included in the measurements can account for the larger size of the apical domain (22.38 Å Stokes radius) determined by sedimentation velocity analysis.

Apical Domain Urea Unfolding Equilibrium Monitored by Bis-ANS Fluorescence. Bis-ANS fluorescence was monitored to follow the urea denaturation of the GroEL apical domain. The thermal reversible folding behavior and the accumulation of an intermediate during equilibrium unfolding of the apical domain in the presence of saturating concentrations of bis-ANS have been reported earlier (*31*). As mentioned above, the apical domain folding intermediate (Figure 1c), which forms at 2.5 M urea, demonstrates increased hydrophobic surface exposure relative to the native apical domain conformation (Figure 1b). In the urea denaturation experiments of the apical domain monitored by bis-ANS fluorescence (Figure 2) at low concentrations of bis-ANS (1 μM, Figure 2, filled squares), there is a maximum bis-ANS fluorescence intensity at ~3.4 M urea. In 5 μM

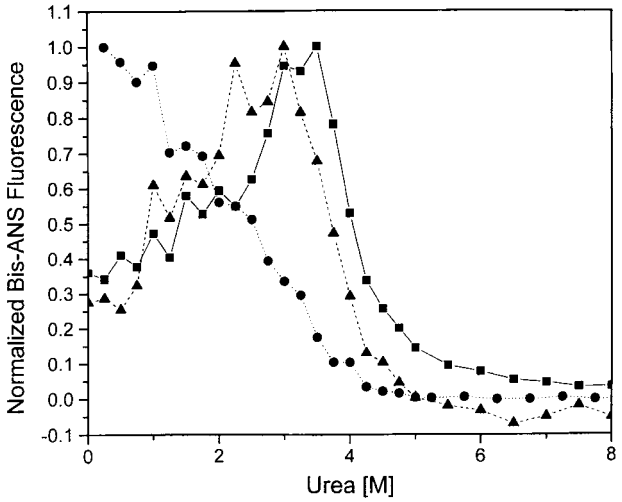

FIGURE 2: Equilibrium denaturation by urea of the GroEL apical domain monitored by bis-ANS fluorescence at 495 nm. Samples of 5 μM apical domain were incubated at a given urea concentration (0.0−8.0 M) with either 1 μM bis-ANS (squares), 5 μM bis-ANS (triangles), or 30 μM bis-ANS (circles) for 20 h in a 10 mM sodium phosphate buffer, pH 7.0. The bis-ANS fluorescence intensity was then measured at 495 nm and plotted as a function of the urea concentration. The data shown have been normalized.

bis-ANS (Figure 2, filled triangles), the maximum shifts only slightly to ~3.3 M urea. At 30 μM bis-ANS (Figure 2, filled circles), the maximum bis-ANS fluorescence shifts to 0 M urea. The similarity in the 1 and 5 μM bis-ANS fluorescence intensity maxima confirms that the apical domain intermediate reaches a maximum accumulation at ~3.4 M urea in the presence of low concentrations of bis-ANS. The maximum bis-ANS fluorescence intensities shift to a lower urea concentration as the bis-ANS concentration increases. The maximum fluorescence observed in the presence of 1 μM bis-ANS at 3.4 M urea is identical to that in the presence of 30 μM bis-ANS without urea (Figure 2). Thus, when bis-ANS concentrations begin to exceed the ratio of 1 mol of bis-ANS per mole of apical domain, the binding of additional molecules of bis-ANS to the apical domain shifts the equilibrium of the native apical domain toward the formation of the apical domain folding intermediate.

Bis-ANS Binds Cooperatively to the Apical Domain. Titration of the apical domain (5 μM) with bis-ANS demonstrated cooperative (sigmoid) binding of bis-ANS (Figure 3). The bis-ANS titration data for the apical domain (squares) were fit by least-squares analysis to the Hill equation (solid line) (eq 1), yielding an apparent binding constant $K \cong 17.36 \pm 0.58$ μM, a Hill coefficient $n \cong 2.00$ ($\pm$0.07), and an $F_{max} \cong (2.8 \pm 0.5) \times 10^5$. The bis-ANS titration data were also analyzed by plots of $[\text{bis-ANS}]_{bound}$ versus $[\text{bis-ANS}]_{free}$ to estimate the total number of bis-ANS molecules bound per apical domain (data not shown). These results allowed us to estimate that 1 mol of apical domain is capable of binding ~7 mol of bis-ANS, in agreement with Golbik et al. (*31*).

The binding of low concentrations of bis-ANS (1−6 μM) to 5 μM apical domain occurred within the dead time of manual mixing (~10 s) (data not shown). When higher concentrations of bis-ANS (12−50 μM) were added to separate solutions containing 5 μM native apical domain, the rates of the bis-ANS binding to the apical domain increased as the bis-ANS concentrations increased (data not shown). A burst phase was observed both for the native and for the urea unfolded (3.5 M) apical domain. The subsequent slower phase is 0.037 $\pm$ 0.001 s^{-1} for the native form and 0.095 $\pm$ 0.01 s^{-1} for the urea unfolded state. This approximately 3-fold rate difference indicates that more hydrophobic exposure is associated with faster binding.

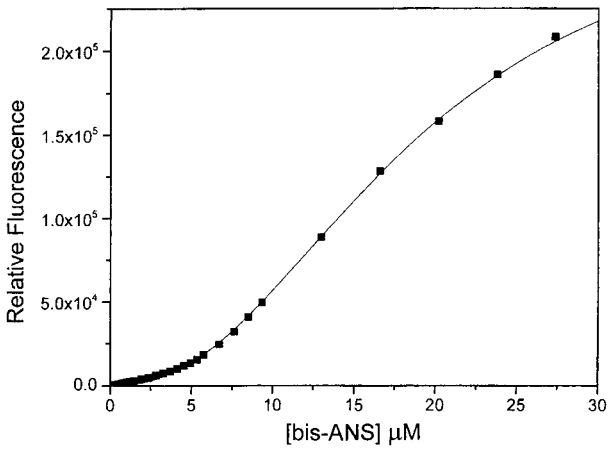

FIGURE 3: Bis-ANS titrations of the GroEL apical domain fragment. 5 μM apical domain was titrated with increasing amounts of bis-ANS (0−30 μM) in a 10 mM sodium phosphate buffer, pH 7.0.

Bis-ANS Binds to GroEL 14mer without Cooperativity and Reveals Two Classes of Binding Sites. To compare the bis-ANS binding characteristics of the apical domain with those of the intact GroEL oligomer, a bis-ANS titration of GroEL (0.357 μM oligomer, ~5 μM apical domain) was performed. The binding of bis-ANS to the GroEL oligomer displays apparent smooth hyperbolic binding (Figure 4b), with much lower bis-ANS fluorescence intensities relative to those observed with the apical domain. The data in Figure 4b were fit using a nonlinear iterative fit to the binding equation (eq 1, where $n = 1$), yielding $K_d \cong 7.44$ μM ($\pm$0.27) and an $F_{max} \cong 9600$ ($\pm$80). The standard deviation among the three experiments was within the area of the symbols.

To convert the direct binding results to provide an estimate of the number of bis-ANS bound per GroEL oligomer, a reverse titration was performed (data not shown). Using eq 1, with $n = 1$, the reverse titration yielded an F_{max} of 11.5 ($\pm$0.37) relative fluorescence units for 0.035 μM bound bis-ANS. The ratio of F_{max} to bound bis-ANS was used to generate the Scatchard plot shown in Figure 4a, which clearly reveals two classes of binding sites. Scatchard data were analyzed using the method of Rosenthal (*46*) and gave results consistent with two different binding sites with a $K_d \cong 0.56$ μM for ~1.7 tight binding sites and a $K_d \cong 10.57$ μM for ~8.5 loose binding sites.

Klotz noted that most Scatchard data, when plotted in a semilog graphic method, could not support the values stated (*47*). When the amount of bound probe is plotted versus the log of the amount of free probe, the experimental data should ideally yield a sigmoidal curve. If the curve has not reached the inflection point, the binding sites have not been saturated, so the transition is not complete and the derived parameters are uncertain. Figure 4c shows that the data obtained in this study have passed the point of inflection, demonstrating that the values obtained are reliable.

Equilibrium Urea Unfolding of the Apical Domain Measured by Tyrosine Fluorescence in the Presence and Absence

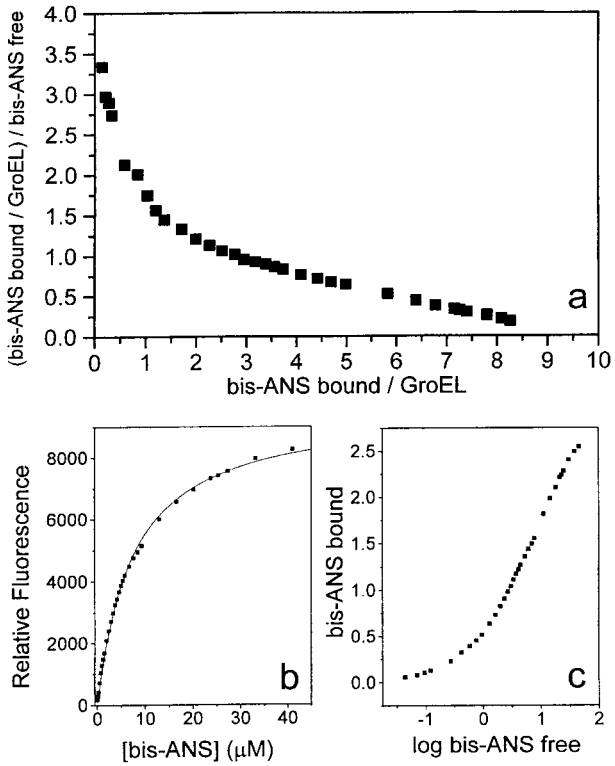

FIGURE 4: Bis-ANS binding to GroEL 14mer. GroEL (0.035 μM, approximately equivalent to 5 μM apical domain) was titrated with increasing amounts of bis-ANS (0−40 μM) in a 10 mM sodium phosphate buffer, pH 7.0. (a) Scatchard plot; (b) direct binding curve; (c) semilog graph of data.

of Bis-ANS. In addition to the formation of the apical domain intermediate at high bis-ANS concentrations, it can also be observed in Figure 2 that the unfolding transition midpoint of the apical domain in going from the intermediate to the denatured state shifts to lower urea concentrations. To further investigate this observation, the intrinsic tyrosine fluorescence was used to monitor the unfolding (Figure 5a−c, filled circles) and the refolding (Figure 5a−c, open circles) of the apical domain (16 μM) in the absence (Figure 5a) and presence of 1 μM (data not shown), 5 μM (Figure 5b), and 30 μM (Figure 5c) bis-ANS. The data for tyrosine fluorescence without bis-ANS and with 1 μM bis-ANS were nearly identical. The data in the absence of 1 μM bis-ANS are discussed here. The unfolding and refolding of 5 μM apical domain were attempted in the presence of bis-ANS, but, due to low signal from the low protein concentration, the data were widely scattered and were not suitable for analysis using either the two- or the three-state equations (eqs 2 and 3). Parameters obtained for 5 and 16 μM apical domain without bis-ANS matched within error. The tyrosine fluorescence was measured at 16 μM apical domain. The intrinsic tyrosine fluorescence intensities decrease on unfolding of the apical domain with urea. The fluorescence data were fit using a two-state transition model and a three-state transition model (data not shown). Fits for the three-state model increased the Chi^2 and will not be used for further discussion. The lines shown in Figure 5a,b represent the fits of unfolding data to the two-state equation. In Figure 5c, the dotted and solid lines are fits to the unfolding and refolding data, respectively. The two-state model gives the parameters y_f, y_u, m_f, m_u, m, and $\Delta G_{(H2O)}$ (eq 2) (*43*). Dividing $\Delta G_{(H2O)}$ by the slope gives an approximate value for the midpoint of

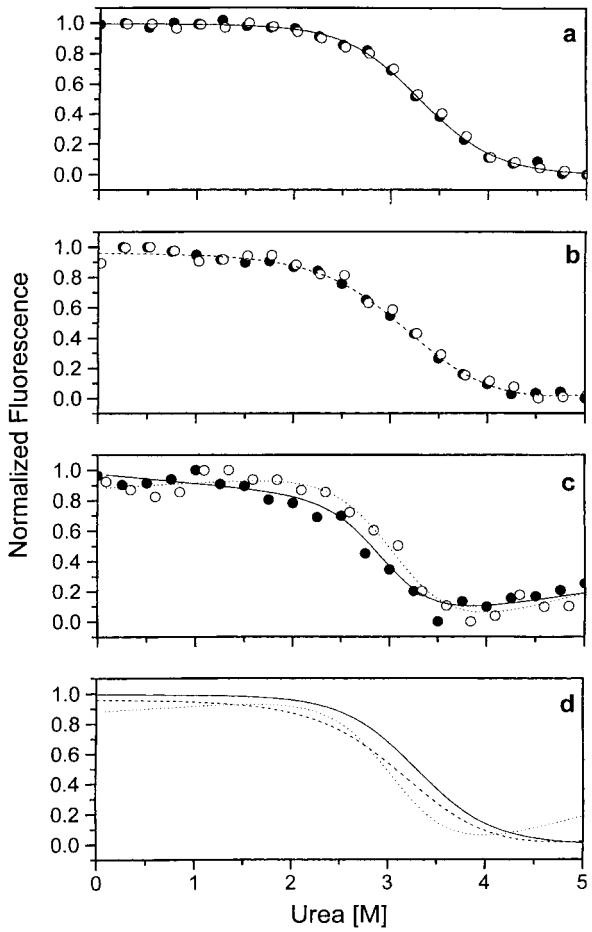

FIGURE 5: Denaturation by urea of the GroEL apical domain monitored by intrinsic tyrosine fluorescence. The unfolding (solid circles) and refolding (open circles) of samples of 16 μM apical domain were incubated at a given urea concentration (0.0−5.0 M) for 24 h in a 10 mM sodium phosphate buffer, pH 7.0. The intrinsic tyrosine fluorescence intensity was then measured at 302 nm and plotted as a function of the urea concentration. The lines are fits (eq 2) to the combined data on unfolding and refolding for panels a and b. The solid line is the fit (eq 2) to the unfolding data for panel c. The dotted line in panel c depicts the fit (eq 2) to the refolding data. Panel d shows the fitted line from panels a and b, and the unfolding data from panel c.

the unfolding transition, called the $U_{1/2}$ or $[D]_{50\%}$. $U_{1/2}$ values obtained were 3.29 ± 0.87 M urea [$\Delta G_{(H2O)} = 5.20 \pm 0.66$ kcal mol^{-1}, $m = 1.58 \pm 0.22$] for the unfolding with no bis-ANS, 3.47 ± 0.95 M urea [$\Delta G_{(H2O)} = 4.86 \pm 1.39$ kcal mol^{-1}, $m = 1.40 \pm 0.45$] for the unfolding with 5 μM bis-ANS, and 2.88 ± 1.08 M urea for the unfolding with 30 μM bis-ANS. The slope (m) of the transition from native (N) to unfolded (U) is related to the difference in solvent-accessible surface area between these two states (*48*). These data suggest that both in the absence of bis-ANS and with 5 μM bis-ANS, the urea unfolding transition for the apical domain corresponds to the transition N ↔ I ↔ U (Figure 2, squares and triangles). However, at 30 μM bis-ANS, only the unfolding of the apical domain intermediate (I ↔ U) is being detected.

Apical Domain Unfolding As Measured by Circular Dichroism. The ellipticities at 222 nm from the CD spectra of the apical domain in the presence of increasing urea were measured (Figure 6). The loss of secondary structure occurs between 2.5 and 4.3 M urea. Furthermore, the urea denaturation of the apical domain monitored by bis-ANS fluo-

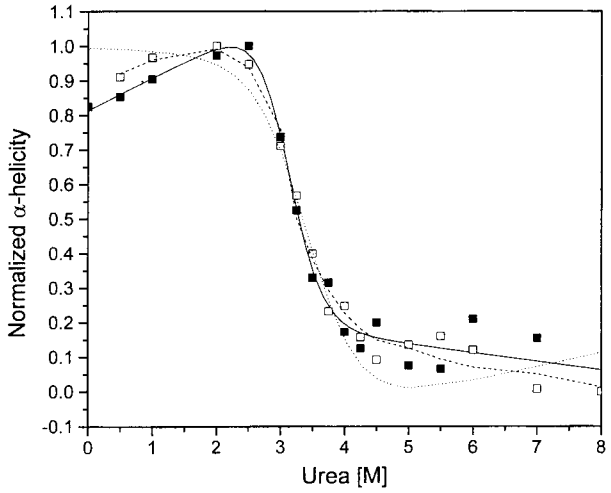

FIGURE 6: Circular dichroism measurements for the apical domain. The ellipticities at 222 nm were measured from experiments described under Materials and Methods. The solid line is a two-state fit of the unfolding data (filled squares). The dashed line is a two-state fit of the refolding data (open squares). The dotted line is the two-state fit of the data for 5 μM unfolding measured by tyrosine fluorescence (data not shown). The close fits indicate that the results from the two different techniques are not very different from each other when random errors are taken into account.

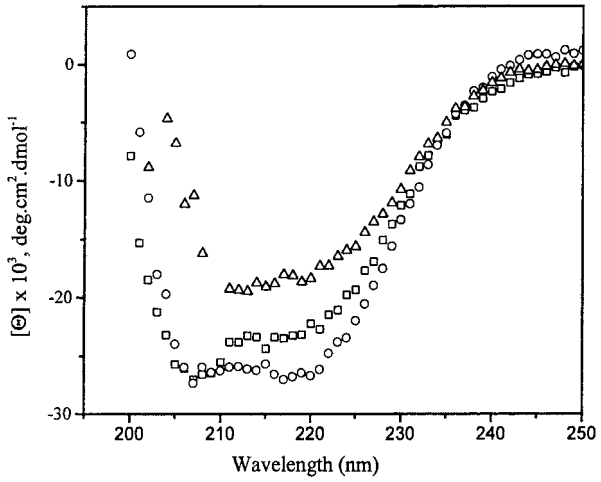

FIGURE 7: Circular dichroism spectra of 5 μM apical domain (open circles), 5 μM apical domain + 30 μM bis-ANS incubated for 5 h (open squares), and 5 μM apical domain in 3.0 M urea for 24 h (open triangles) as described under Materials and Methods. The reaction conditions were 10 mM sodium phosphate, pH 7.0, buffer at $T = 25$ °C.

rescence at low bis-ANS concentrations (Figure 2), which most defensibly corresponds to the CD data acquired in the absence of bis-ANS, still retains considerable hydrophobic surface exposure at 3.0 M urea. These data were fit with a two-state (Figure 6, unfolding, solid line; refolding, dashed line) and three-state model (data not shown). The three-state fit did not significantly change the parameters or decrease the residuals or Chi^2. The $U_{1/2}$ value for the unfolding/refolding detected by CD was 3.30 M urea. These data fit very closely to the urea unfolding values obtained by following the tyrosine fluorescence (Figure 6, dotted line). The overlaid spectra of 5 μM apical domain only, 5 μM apical domain incubated with 30 μM bis-ANS, and 5 μM apical domain unfolded for 24 h in 3.0 M urea are shown in Figure 7. It is evident that in the presence of excess bis-ANS there is only a small decrease in the secondary structure (Figure 7, open squares), and there is still a significant amount of secondary structure present at 3.0 M urea (Figure 7, open triangles). These observations of the apical domain at 3.0 M urea are similar to the properties associated with a "molten globule" intermediate: retained secondary structure (CD), and significant accessibility of hydrophobic surfaces (bis-ANS fluorescence) (*49, 50*). Attempts were made to obtain CD spectra in the near-UV region (250−350 nm) using a 1.0 cm path length cell. However, the ellipticities observed in this region (1.0 cm path length cell) are completely masked by the high absorbance of the protein solution (5 μM) containing 30 μM bis-ANS. Using a higher concentration of the protein at the desired stoichiometry (1:6 apical domain:bis-ANS ratio) in a less than 1.0 cm path length cell also led to similar technical difficulties.

DISCUSSION

GroEL binds a variety of substrate polypeptides in their non-native conformations (*15, 51, 52*), and several studies have suggested the importance of hydrophobicity in these interactions (*16, 17, 34, 53*−*58*). The GroEL crystal structure (*8*) and mutational analysis (*11*) have suggested that the site of GroEL substrate polypeptide interactions occurs at hydrophobic residues located in the apical domain of GroEL. However, when hydrophobic surfaces on GroEL were probed with bis-ANS, only one to two molecules of the probe were bound tightly per GroEL oligomer (*53*). Divalent cations and positively charged amphipathic peptides have been shown to increase the GroEL hydrophobic surface exposure when bound (*55, 56, 59*). These data suggest that the maximum binding of substrate polypeptide to GroEL is favored by a combination of substrate charge and hydrophobicity.

The crystal structure of the apical domain fragment (191−345) with the N-terminal 17-residue histidine tag has been shown to be virtually identical to that of the apical domain in the intact GroEL oligomer (*28*). We have utilized this monomeric GroEL apical domain fragment [sht-GroEL (191−345)] to study the hydrophobic characteristics of the apical domain in the absence of the intact GroEL quaternary structure and its associated allosteric properties. The apical domain displays cooperative binding of bis-ANS. Low concentrations of bis-ANS (Figure 2, 1 μM, filled squares; and 5 μM, filled triangles) show the formation of an intermediate at about 3.0 M urea during urea unfolding. At high concentrations of bis-ANS (30 μM), the bis-ANS-bound protein in the absence of urea resembles the intermediate as seen from its fluorescence intensity (Figure 2, filled circles). The thermodynamic stability and folding of the apical domain fragment (191−345) were previously taken to indicate reversible folding of the native apical domain relative to the unfolded state (*31*). Our data suggest that the apparent stabilization of the apical domain is not the free energy of the native apical domain relative to the denatured apical domain transition (N $\leftrightarrows$ U), but rather the free energy of the apical domain intermediate relative to the unfolded apical domain (I $\leftrightarrows$ U), since in the previous study saturating concentrations of bis-ANS (40 μM) were used (*31*).

Almost all models to date implicitly assume that en bloc movements of apical domains are responsible for exposing interactive sites on GroEL. If this were the case, GroEL apical domains should have the most hydrophobic surface

exposure in the unperturbed state. However, it has been demonstrated in this study that the apical domains contain relatively little hydrophobic surface in the unperturbed state. The exposure of hydrophobic surfaces on the apical domains was only observed upon the addition of increasing bis-ANS concentrations or perturbation with urea. Thus, since the apical domains are monomeric and lack the intermediate and equatorial domains required for oligomerization, the modulation of its hydrophobic surfaces must be due to perturbations of the tertiary structure within the apical domain. These changes in structure could be accomplished in the intact GroEL oligomer by allosteric control mediated by the intermediate domain.

It was observed that the binding of bis-ANS to the apical domain was cooperative, that the binding of bis-ANS destabilized the native apical domain structure, and that the formation of apical domain intermediates was bis-ANS concentration dependent. The equilibrium unfolding of the apical domain monitored by bis-ANS fluorescence (Figure 2) shows that formation of the apical domain intermediate is favored by bis-ANS binding, and suggests that such binding shifts the equilibrium of the native apical domain conformation to the intermediate conformation (*60*).

The apical domain has been demonstrated to facilitate the refolding of both rhodanese and cyclophilin, and to catalyze the unfolding of barnase (*28*), implying that at least a transient complex can form between these species. The GroEL 14mer forms an extremely tight complex with rhodanese in the absence of nucleotides or GroES, a process that stabilizes the GroEL 14mer (*61*). Similarly, the co-chaperonin GroES in the presence of ATP−Mg^{2+} binds tightly to GroEL ($K_d \approx 30$ nM) (*62, 63*). These results suggest that, although the apical domain is capable of facilitating the refolding of substrate polypeptides, the tight binding of substrate polypeptides such as rhodanese and the co-chaperonin GroES requires elements of GroEL structure other than that contained within single apical domains. It is plausible to assume that the observed net tight binding of GroEL to substrate polypeptides results from multiple weak interactions of the GroEL apical domains (*64*). Thus, the binding interactions of the apical domains with substrate polypeptides may be individually weak, requiring the multiple binding sites supplied by the intact GroEL 14mer before tight net binding of substrate polypeptides can be detected. This would permit some flexibility of the bound substrate polypeptide by dissociation at some sites, without permitting its release from the complex.

Previous studies using amphipathic peptides suggested that binding to GroEL occurred by hydrophobic association, and that the binding of these peptides to GroEL could induce the formation of increased hydrophobic surfaces on GroEL (*55*). It was confirmed by sedimentation velocity experiments and finite-element analysis that the apical domain is monomeric. Thus, the hydrophobic surfaces on the apical domains are not hidden by self-association, and this demonstrates either that the hydrophobic surfaces on the isolated apical domains are not exposed or that their distribution and/or orientation within the apical domains precludes them from self-association. In addition, the conformational malleability of the apical domain, as seen by the formation of an intermediate at high concentrations of bis-ANS, is not seen in the intact GroEL oligomer. Therefore, this malleability of the isolated apical domain is restricted in the intact oligomeric GroEL. The cause of this restriction could be from two sources: (1) attachment to the intermediate domain, or (2) packing of the apical domain within the oligomeric structure.

Since the apical domain is in the middle of the sequence of a monomer, attachment of the apical domain to the intermediate domain would likely increase the stability of the apical domain and coordinate the overall cooperativity of the hydrophobic exposure within a ring of GroEL. However, it is clear that the induced hydrophobic surfaces of the apical domain cannot be explained completely by simple en bloc movements as described for the intact GroEL 14mer. Thus, it is likely that the observed induced hydrophobic surface exposure reflects the dynamic and flexible movements that can occur within the apical domains of the intact GroEL 14mer.

Furthermore, increased hydrophobic exposure on the monomeric apical domain may not lead to tight polypeptide binding. Thus, a prerequisite for tight substrate polypeptide binding is the presence of all three GroEL domains and the intact GroEL oligomer. The oligomeric architecture of the intact GroEL 14mer and its multiple binding sites within a heptameric ring may be essential components required for tight net binding of substrate polypeptides and their subsequent release. Part of the potential binding energy must be expended in inducing the surfaces in the monomer that could be provided by the other components of the system (i.e., nucleotides, cations, GroES) with the intact GroEL 14mer. The ability of ligands to modulate the exposure of flexible hydrophobic binding surfaces in the apical domains of GroEL may be an important aspect of the binding and release mechanism of substrate polypeptides.

ACKNOWLEDGMENT

We thank Virgil Schirf at the Center for Analytical Ultracentrifugation facility, Department of Biochemistry, University of Texas Health Science Center at San Antonio, TX, for his help in analyzing the XLA data.

REFERENCES

1. Ellis, R. J., and van der Vies, S. M. (1991) *Annu. Rev. Biochem. 60*, 321−347.
2. Ellis, R. J., and Hartl, F. U. (1999) *Curr. Opin. Struct. Biol. 9*, 102−110.
3. Horwich, A. L., Weber-Ban, E. U., and Finley, D. (1999) *Proc. Natl. Acad. Sci. U.S.A. 96*, 11033−11040.
4. Agashe, V. R., and Hartl, F. (2000) *Semin. Cell Dev. Biol. 11*, 15−25.
5. Gottesman, M. E., and Hendrickson, W. A. (2000) *Curr. Opin. Microbiol. 3*, 197−202.
6. Viitanen, P. V., Gatenby, A. A., and Lorimer, G. H. (1992) *Protein Sci. 1*, 363−369.
7. Hendrix, R. W. (1979) *J. Mol. Biol. 129*, 375−392.
8. Braig, K., Otwinowski, Z., Hegde, R., Boisvert, D. C., Joachimiak, A., Horwich, A. L., and Sigler, P. B. (1994) *Nature 371*, 578−586.
9. Braig, K., Adams, P. D., and Brunger, A. T. (1995) *Nat. Struct. Biol. 2*, 1083−1094.
10. Boisvert, D. C., Wang, J., Otwinowski, Z., Horwich, A. L., and Sigler, P. B. (1996) *Nat. Struct. Biol. 3*, 170−177.
11. Fenton, W. A., Kashi, Y., Furtak, K., and Horwich, A. L. (1994) *Nature 371*, 614−619.

12. Chen, S., Roseman, A. M., Hunter, A. S., Wood, S. P., Burston, S. G., Ranson, N. A., Clarke, A. R., and Saibil, H. R. (1994) *Nature 371*, 261−264.
13. Seale, J. W., Martinez, J. L., and Horowitz, P. M. (1995) *Biochemistry 34*, 7443−7449.
14. Seale, J. W., Brazil, B. T., and Horowitz, P. M. (1998) *Methods Enzymol. 290*, 318−323.
15. Buchner, J., Schmidt, M., Fuchs, M., Jaenicke, R., Rudolph, R., Schmid, F. X., and Kiefhaber, T. (1991) *Biochemistry 30*, 1586−1591.
16. Shtilerman, M., Lorimer, G. H., and Englander, S. W. (1999) *Science 284*, 822−825.
17. Wang, Z., Feng, H., Landry, S. J., Maxwell, J., and Gierasch, L. M. (1999) *Biochemistry 38*, 12537−12546.
18. Wang, J. D., and Weissman, J. S. (1999) *Nat. Struct. Biol. 6*, 597−600.
19. Chen, J., and Smith, D. L. (2000) *Biochemistry 39*, 4250−4258.
20. Weissman, J. S., Rye, H. S., Fenton, W. A., Beechem, J. M., and Horwich, A. L. (1996) *Cell 84*, 481−490.
21. Chatellier, J., Buckle, A. M., and Fersht, A. R. (1999) *J. Mol. Biol. 292*, 163−172.
22. Wang, J. D., Michelitsch, M. D., and Weissman, J. S. (1998) *Proc. Natl. Acad. Sci. U.S.A. 95*, 12163−12168.
23. Weber, F., Keppel, F., Georgopoulos, C., Hayer-Hartl, M. K., and Hartl, F. U. (1998) *Nat. Struct. Biol. 5*, 977−985.
24. Hayer-Hartl, M. K., Ewalt, K. L., and Hartl, F. U. (1999) *J. Biol. Chem. 380*, 531−540.
25. Nielsen, K. L., and Cowan, N. J. (1998) *Mol. Cells 2*, 93−99.
26. Erbse, A., Yifrach, O., Jones, S., and Lund, P. A. (1999) *J. Biol. Chem. 274*, 20351−20357.
27. Jarabak, R., Westley, J., Dungan, J. M., and Horowitz, P. (1993) *J. Biochem. Toxicol. 8*, 41−48.
28. Zahn, R., Buckle, A. M., Perrett, S., Johnson, C. M., Corrales, F. J., Golbik, R., and Fersht, A. R. (1996) *Proc. Natl. Acad. Sci. U.S.A. 93*, 15024−15029.
29. Taguchi, H., Makino, Y., and Yoshida, M. (1994) *J. Biol. Chem. 269*, 8529−8534.
30. Makino, Y., Taguchi, H., and Yoshida, M. (1993) *FEBS Lett. 336*, 363−367.
31. Golbik, R., Zahn, R., Harding, S. E., and Fersht, A. R. (1998) *J. Mol. Biol. 276*, 505−515.
32. Chatellier, J., Hill, F., Lund, P. A., and Fersht, A. R. (1998) *Proc. Natl. Acad. Sci. U.S.A. 95*, 9861−9866.
33. Buckle, A. M., Zahn, R., and Fersht, A. R. (1997) *Proc. Natl. Acad. Sci. U.S.A. 94*, 3571−3575.
34. Tanaka, N., and Fersht, A. R. (1999) *J. Mol. Biol. 292*, 173−180.
35. Kobayashi, N., Freund, S. M., Chatellier, J., Zahn, R., and Fersht, A. R. (1999) *J. Mol. Biol. 292*, 181−190.
36. Miller, D. M., Kurzban, G. P., Mendoza, J. A., Chirgwin, J. M., Hardies, S. C., and Horowitz, P. M. (1992) *Biochim. Biophys. Acta 1121*, 286−292.
37. Staniforth, R. A., Cortes, A., Burston, S. G., Atkinson, T., Holbrook, J. J., and Clarke, A. R. (1994) *FEBS Lett. 344*, 129−135.
38. Clark, A. C., Hugo, E., and Frieden, C. (1996) *Biochemistry 35*, 5893−5901.
39. van Holde, K. E., and Weischet, W. O. (1978) *Biopolymers 17*, 1387−1403.
40. Demeler, B. (1998) http://www.biochem.uthscsa.edu/UltraScan.
41. Sober, H. (1968) *The Handbook of Biochemistry and Molecular Biology*, Chemical Rubber Co., Cleveland, OH.
42. Lakowicz, J. R. (1983) *Principles of Fluorescence Spectroscopy*, Plenum Press, New York.
43. Santoro, M. M., and Bolen, D. W. (1988) *Biochemistry 27*, 8063−8068.
44. Sun, T. X., Akhtar, N. J., and Liang, J. J. (1999) *J. Biol. Chem. 274*, 34067−34071.
45. Demeler, B., and Saber, H. (1998) *Biophys. J. 74*, 444−454.
46. Rosenthal, H. E. (1967) *Anal. Biochem. 20*, 525−532.
47. Klotz, I. M. (1982) *Science 217*, 1247−1249.
48. Schellman, J. A. (1978) *Biopolymers 17*, 1305−1322.
49. Kuwajima, K. (1989) *Proteins: Struct., Funct., Genet. 6*, 87−103.
50. Ptitsyn, O. B., Pain, R. H., Semisotnov, G. V., Zerovnik, E., and Razgulyaev, O. I. (1990) *FEBS Lett. 262*, 20−24.
51. Mendoza, J. A., Rogers, E., Lorimer, G. H., and Horowitz, P. M. (1991) *J. Biol. Chem. 266*, 13044−13049.
52. Viitanen, P. V., Lubben, T. H., Reed, J., Goloubinoff, P., O'Keefe, D. P., and Lorimer, G. H. (1990) *Biochemistry 29*, 5665−5671.
53. Horowitz, P. M., Hua, S., and Gibbons, D. L. (1995) *J. Biol. Chem. 270*, 1535−1542.
54. Lin, J., and Ficht, T. A. (1995) *Infect. Immun. 63*, 1409−1414.
55. Brazil, B. T., Cleland, J. L., McDowell, R. S., Skelton, N. J., Paris, K., and Horowitz, P. M. (1997) *J. Biol. Chem. 272*, 5105−5111.
56. Brazil, B. T., Ybarra, J., and Horowitz, P. M. (1998) *J. Biol. Chem. 273*, 3257−3263.
57. Zahn, R., Axmann, S. E., Rucknagel, K. P., Jaeger, E., Laminet, A. A., and Pluckthun, A. (1994) *J. Mol. Biol. 242*, 150−164.
58. Zahn, R., Spitzfaden, C., Ottiger, M., Wuthrich, K., and Pluckthun, A. (1994) *Nature 368*, 261−265.
59. Gorovits, B. M., Ybarra, J., and Horowitz, P. M. (1997) *J. Biol. Chem. 272*, 6842−6845.
60. Shi, L., Palleros, D. R., and Fink, A. L. (1994) *Biochemistry 33*, 7536−7546.
61. Mendoza, J. A., and Horowitz, P. M. (1994) *J. Biol. Chem. 269*, 25963−25965.
62. Gorovits, B. M., Ybarra, J., Seale, J. W., and Horowitz, P. M. (1997) *J. Biol. Chem. 272*, 26999−27004.
63. Behlke, J., Ristau, O., and Schonfeld, H. J. (1997) *Biochemistry 36*, 5149−5156.
64. Brazil, B. T., and Horowitz, P. M. (1999) *Cell Stress Chaperones 4*, 177−190.

BI001822B